Numerical Simulation of the 29 November 1975 Island of Hawaii Tsunami by the Finite-Element Method[1]

MICHAEL A. SKLARZ,[2] LESTER Q. SPIELVOGEL[3] AND HAROLD G. LOOMIS[3]

Joint Institute for Marine and Atmospheric Research, University of Hawaii, Honolulu 96822

(Manuscript received 10 July 1978, in final form 7 May 1979)

ABSTRACT

The finite-element method is applied to study the transient response of a locally generated tsunami. The model time-steps the linearized shallow-water wave equation over a variable mesh of triangular and quadrilateral elements. Actual bathymetry is used. Numerical results are obtained for a simulation of the 1975 tsunami which occurred off the southeast coast of the island of Hawaii.

Attention is focused on properly representing the initial tsunami disturbance as well as qualitative and quantitative comparisons of predicted-to-observed wave heights. These comparisons support the viability of the finite-element method for such tsunami applications.

1. Introduction

Tsunamis are gravity waves resulting from large-scale, short-duration disturbances of the ocean. They are typically generated by tectonic earthquakes but may also be associated with coastal and submarine landslides, volcanic eruptions, or man-made nuclear explosions. The ratio of the length of the disturbance or radius of curvature of the water surface to water depth is typically large. Thus, tsunamis fall under the classification of long waves, and shallow-water theory generally gives a good approximation to actual occurrences.

Numerous analytic theories of tsunami generation and propagation are available. Due to the difficult mathematical nature of this problem, these studies are restricted to simplified bathymetries and geometries. Kranzer and Keller (1959) derive expressions for wave elevations produced by explosions either above or below the water surface. They consider a water body of constant depth. Only their farfield (large distance from initial disturbance) solutions are valid as they make use of the method of stationary phase. Tuck and Hwang (1972) present a general solution of the linear shallow-water equations for arbitrary ground motion on a sloping beach. Spielvogel (1975) derives analytic solutions of the nonlinear shallow-water equations for various initial surface displacements. Particular attention is given to the relationship between wave amplitude at the shoreline and wave runup height.

Numerical modelling allows for the inclusion of more realistic initial disturbances and bathymetries. Reid and Vastano (1966) use a conformal mapping technique and develop an "island coordinate system" suitable for the analysis of long gravity waves near islands. Hwang and Divoky (1970) numerically simulate the tsunami generation and propagation following the 1964 Alaskan earthquake. Based on a finite-difference method (FDM) scheme adapted from Leedertse (1967) they time step and nonlinear shallow-water equations over a variable depth spherical polar coordinate grid. Chen (1973) also simulates the 1964 tsunami by the FDM and develops a suitable open-sea boundary condition analogous to the matched impedence boundary condition used in acoustic radiation. Mader (1974) models tsunami interaction with continental slopes and shelves by time stepping the two-dimensional, nonlinear, incompressible, viscous, Navier-Stokes equations using the Marker and Cell method. Taylor and Davis (1974) apply the finite element method (FEM) to time step the nonlinear shallow-water equations to study tidal propagation in estuaries and open seas. Houston (1978) applies the FEM to study the interaction of time-harmonic long waves with the Hawaiian Islands. He uses a hybrid finite-element model originally developed for harbor oscillation and wave scattering problems by Chen and Mei (1974).

In this study the finite-element method (FEM) is used to simulate the transient response of a locally generated tsunami, in particular the 29 November 1975 tsunami which occurred off the southeast

[1] Contribution No. 363 from NOAA/ERL Pacific Marine Environmental Laboratory. Contribution No. 964 from Hawaii Institute of Geophysics, University of Hawaii.

[2] Project No. NRC-04-77-047.

[3] Pacific Marine Environmental Laboratory, NOAA, Seattle, WA.

0022-3670/79/051022-10$06.50

coast of the island of Hawaii. For such an application the FEM offers a number of advantages over commonly used Cartesian or polar grid finite-difference methods.

First, a finite-element mesh allows for a good representation of an irregular boundary such as an island coastline. By using combinations of triangular and quadrilateral elements the simulated region can be shaped to conform to highly irregular geometries.

Second, the mesh may be refined locally. Thus, different levels of emphasis may be given to areas where more detail is desired (e.g., in the tsunami source region or along the shoreline where comparisons of predicted and measured wave heights are to be made) or required (e.g., in regions of more irregular geometry or bathymetry).

Third, the finite-element method is well suited for incorporating boundary conditions. Boundary conditions appear as boundary integrals generated naturally in the problem formulation.

This paper is organized in four sections. First, the hydrodynamic and corresponding mathematical theory is presented. Second, the solution to the problem is formulated via the finite-element method. Third, a brief discussion of the tsunami source mechanism and inferred model initial conditions is made. Finally, numerical predictions and actual measurements are compared.

2. Theory

It is assumed that a tsunami acts as a shallow-water wave. In the event there is no wave breaking, bore formation, nearshore stratification, or significant frictional effects, linearized shallow water theory is valid leading to the classical linearized long-wave equation,

$$L[\eta(x,y,t)] = \frac{\partial^2 \eta}{\partial t^2} - g\nabla\cdot(h\nabla\eta) = 0. \qquad (1)$$

Here η is the free-surface elevation above the equilibrium level, t time, h the local still-water depth, g the acceleration of gravity, and ∇ the horizontal-gradient operator.

Along the island coastline we require a zero net flux of energy (i.e., total reflection). Thus,

$$(\mathbf{n}\cdot\nabla\eta)h = 0, \qquad (2)$$

where $\mathbf{n}$ is a horizontal unit vector normal to the island boundary. In the present model it is assumed that the shoreline is a vertical barrier with h = 9.13 m (30 ft) thus requiring

$$\frac{\partial \eta}{\partial n} = 0. \qquad (3)$$

Along the open boundary of the mesh it is necessary to insure that only outgoing waves are present so that all energy is radiated outward. When a plane wave encounters a fixed boundary (Dirichlet condition) the reflection is equal in magnitude but opposite in sign to that from a free boundary (Neumann condition). Thus, the average of the two solutions should correspond to a perfectly (exact to roundoff) transmitting boundary for the earliest reflected waves. For straight boundaries, this has been demonstrated by Smith (1974). In the general linear problem there will be multiple-boundary reflections requiring additional solutions to be averaged, thus making the method computationally inefficient. For the present tsunami simulation, however, this technique is quite appropriate as the motion is started impulsively and only a limited time history is of interest.

3. Finite-element formulation

The finite-element representation of (1) is obtained by the method of weighted residuals with the Galerkin criterion in the selection of the weighting function (e.g., Zienkiewicz, 1971). This method assumes that for each element an approximate representation, $\tilde{\eta}^e(x,y,t)$, for the dependent variable will be chosen. The global trial function $\tilde{\eta}$ is defined as the composition of the local (defined within an element) trial functions

$$\tilde{\eta}^e(x,y,t) = \sum_{j=1}^{r} N_j^e(x,y)\eta_j(t), \qquad (4)$$

where e refers to the element index, j refers to the r nodes (in the element or "local" indexing system) of the element, $\eta_j(t)$ are the unknown nodal values of the dependent variable, and the coefficients $N_j^e \times (x,y)$ are known functions of the x and y coordinates and are termed "shape functions." Substituting the approximate solution (4) into the governing differential equation (1) yields

$$L[\tilde{\eta}(x,y,t)] = R \neq 0, \qquad (5)$$

where R is a residual value. The governing differential equation cannot be satisfied pointwise throughout the domain but the residual can be minimized in a weighted-average sense, i.e.,

$$\iint_A L[\tilde{\eta}]\Omega_i(x,y)dA = 0 \quad \text{for all} \quad i, \qquad (6)$$

where Ω_i is a weighting function and the integration is performed over the domain. In the Galerkin form of this weighted residual method, the shape functions $N_i(x,y)$ are substituted for Ω_i. Each shape function then leads to a distinct algebraic equation.

Substituting (4) into (1) and following (6), we obtain in each element indexed by (e)

$$\iint_{A^{(e)}} N_i^{(e)}(x,y)L[\sum_{j=1}^{r} N_j^{(e)}(x,y)\eta_j(t)]dxdy = 0,$$

$$i = 1, r. \tag{7}$$

Integrating by parts and introducing the boundary terms in the resulting integral leads to a system of algebraic equations for each element

$$\sum_{j=1}^{r} k_{ij}^{(e)} \eta_j(t + \Delta t) = b_i^{(e)}, \tag{8}$$

where

$$k_{ij}^{(e)} = \iint_{A^{(e)}} [N_i^{(e)} N_j^{(e)} + \tfrac{1}{2} g(\Delta t)^2 h^{(e)} \nabla N_i^{(e)} \cdot \nabla N_j^{(e)}] dx dy, \tag{9}$$

$$b_i^{(e)} = \iint_{A^{(e)}} \{N_i^{(e)}[2 \sum_{j=1}^{r} N_j^{(e)} \eta_j(t) - \sum_{j=1}^{r} N_j^{(e)} \eta_j(t - \Delta t)]$$

$$- \tfrac{1}{2} g(\Delta t)^2 h^{(e)} \nabla N_i^{(e)} \cdot \sum_{j=1}^{r} \nabla N_j^{(e)} \eta_j(t)\} dx dy + g(\Delta t)^2 \int_{\partial A^{(e)}} h^{(e)} N_i^{(e)} \frac{\partial \bar{\eta}}{\partial n} dl^{(e)}. \tag{10}$$

Here $h^{(e)}$ is the depth of element (e) and $\partial \bar{\eta}/\partial n$ is the derivative of $\bar{\eta}$ in the direction of the exterior normal to the element boundary $l^{(e)}$. We have used the approximations

$$\frac{\partial^2 \bar{\eta}}{\partial t^2} \approx \sum_{j=1}^{r} N_j(x,y) \left[\frac{\eta_j(t + \Delta t) + 2\eta_j(t) + \eta_j(t - \Delta t)}{(\Delta t)^2} \right], \tag{11}$$

$$\nabla \bar{\eta} \approx \sum_{j=1}^{r} \nabla N_j(x,y)[\tfrac{1}{2}\eta_j(t) + \tfrac{1}{2}\eta_j(t + \Delta t)]. \tag{12}$$

The decision for such a time average of the gradient term is based on extensive numerical experiments in which the one-dimensional wave equation for a square-wave (tsunami-like) initial condition was time stepped over a flat bottom of representative depth 500 m. The gradient term was approximated in numerous ways with the arrangement in Eq. (12) giving the overall best correlation of wave form and arrival time to the well-known D'Alembert solution. Other numerical experiments were performed, also with positive results in one and two dimensions with variable bathymetry as a check on compatability and model error generation of this method. The calculations are unconditionally stable since the scheme is implicit in time. The test cases demonstrated that for the times and distances involved in this simulation there should be no misleading effects due to dispersion.

The equations of the entire domain are constructed from the equations of the elements by requiring η to be continuous at each element node. The significance of this condition is that all coefficients $k_{ij}^{(e)}$ and $b_i^{(e)}$ with like global subscripts are simply added leading to a global system of n algebraic equations in the n unknowns η_i.

$$[K]\boldsymbol{\eta}(t + \Delta t) = \mathbf{B}, \tag{13}$$

where

$$K_{i'j'} = \sum_{e=1}^{ne} k_{ij}^{(e)}, \quad B_{i'} = \sum_{e=1}^{ne} b_i^{(e)}, \tag{14}$$

and the summations range over all (ne) elements. Note that the right-side and left-side (primed) indices refer to the local and global coordinate systems, respectively.

Guided by the results of the above mentioned numerical experiments, the time step (Δt) for this simulation is taken to be 7.5 s. Smaller time steps give similar results while the results for time steps of 15 s or more are stable but inaccurate.

4. Elements

Following previous studies (Zienkiewicz, 1972), quadratic shape functions (serendipity family for quadrilateral elements) are used as, in general, a quadratic description of both element geometry and assumed dependent variable representation offers the optimal mix of accuracy and efficiency. Although the element sides are not curved in this study such a feature may be readily included.

The mesh of six-noded triangular (39) and eight-noded quadrilateral (99) elements is shown in Fig. 1. The choice of this element configuration reflects the following various considerations:

1) The island boundary is accurately represented.

2) The maximum wave travel time across an element is approximately constant.

3) There is greater detail along the shoreline and above the tsunami source region.

4) The necessary number of nodes (443) and the bandwidth (42) of the algebraic equations (8) to be solved is kept to a reasonable minimum. This reduced bandwidth is made possible by not enclosing the mesh on the north side of the island. Reflections from these artificial boundaries do not interfere with the primary waves for the times and sites of interest.

A technique to avoid spurious hills and valleys arising from the quadratic representation of the bathymetry is discussed in the Appendix. Nodal depths are taken from Coast and Geodetic Survey Chart 4102.

5. Tsunami source mechanism

The transient tsunami response is intimately dependent on the specific features of the generating earthquake. In general, this ground motion is quite complex and a time history may only be inferred for a particular tsunami. For a very large earthquake (1964, Alaskan) the corresponding ground motion and, thus tsunami source mechanism, may be better understood by virtue of the number of seismic stations affected and the extensive ensuing crustal dislocation. The 1975 earthquake is quite small by comparison. Thus, details of the tectonic displacement are not well understood. Furumoto and Kovach (1977) are presently gathering available data to shed some light on this problem. On the basis of initial data they suggest a displacement of the island shelf to uplift the water

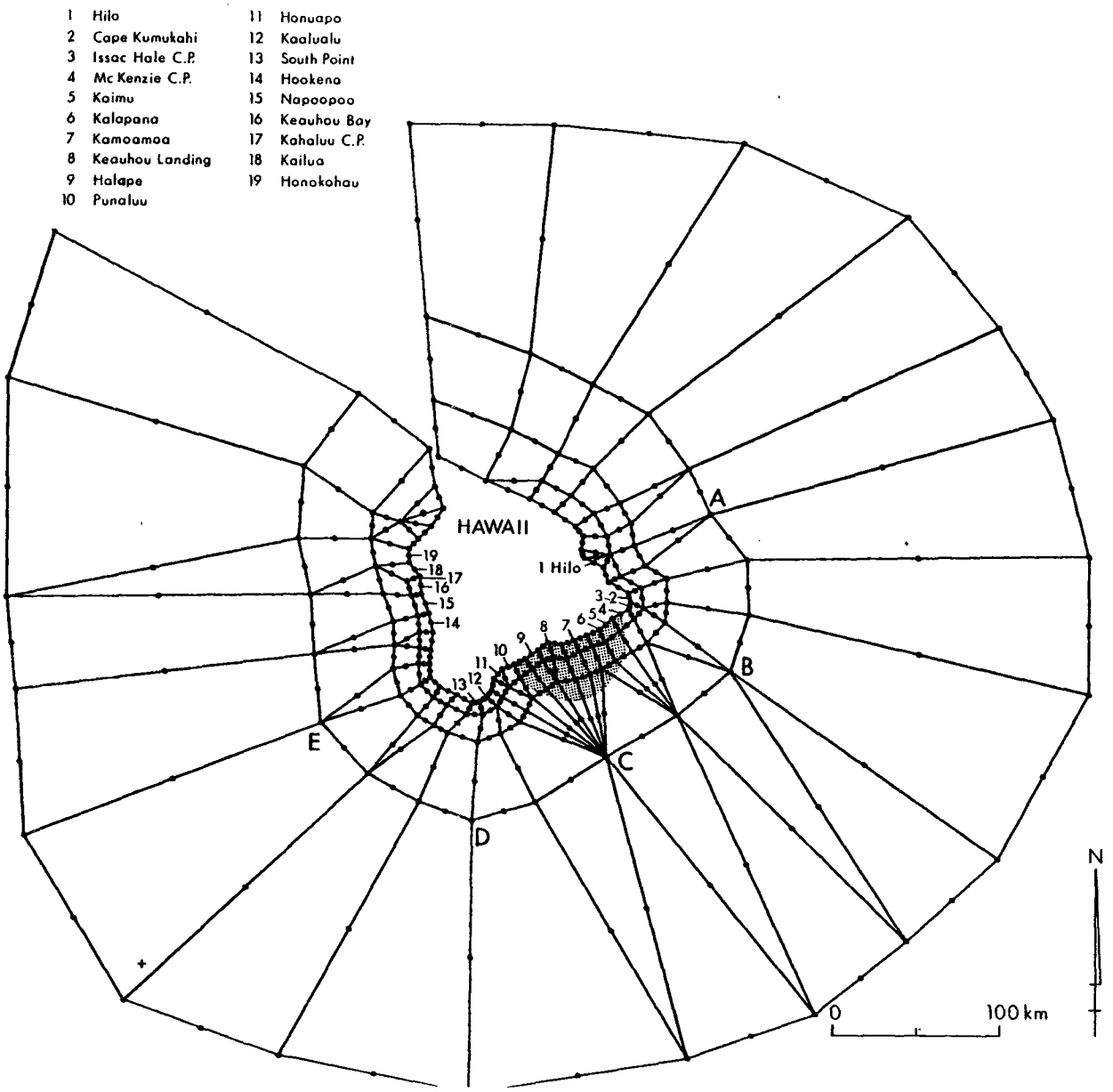

FIG. 1. Finite element mesh and node locations as designed for 29 November 1975 Island of Hawaii tsunami. Shaded area corresponds to the region of ocean bottom assumed to have been uplifted. Numbers refer to coastal locations as listed, letters to offshore sites of interest; both are referred to in subsequent figures.

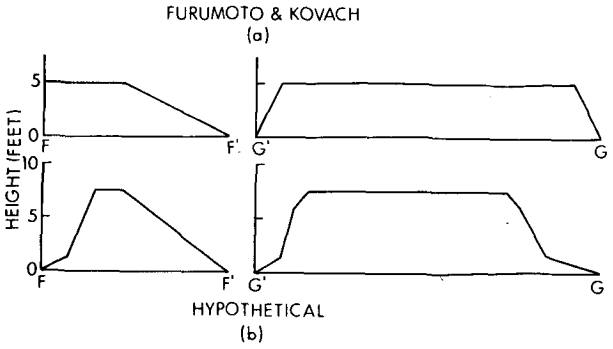

FIG. 2. Proposed cross sections of initial uplift of water above MSL. Potential energy of (b) is approximately 85% that of (a). Here lines are drawn connecting the specified nodal values. In the numerics a similar polynomial surface is fit.

column contained within the shaded region in Fig. 1. The extent of this uplift is in close agreement with that determined by Hatori (1976).

Numerical experiments with the linearized long-wave equation suggest that such a ground motion may be interpreted as being equivalent to an initial elevation of the free surface. This result was also derived for farfield characteristics of the resulting tsunami in a previous paper by Tuck and Hwang (1972) and demonstrated experimentally by Hammack (1972).

Thus, as a first simulation of the 1975 tsunami the initial wave elevation, $\eta(x,y,0)$, is specified as 5 ft at all nodes situated on the uplift region and zero everywhere else. Cross sections of the uplift as specified are shown in Fig. 2a. Here straight lines are drawn between nodel values. In the numerics a similar polynomial surface is fit as discussed in Section 4. The initial velocity, $\partial\eta(x,y,0)/\partial t$, is presumed zero at all nodes.

6. Numerical results

The predicted transient tsunami response to the Furumoto and Kovach source is shown at various coastal and offshore sites in Figs. 3–6. The coastal site amplitudes have been multiplied by a factor of

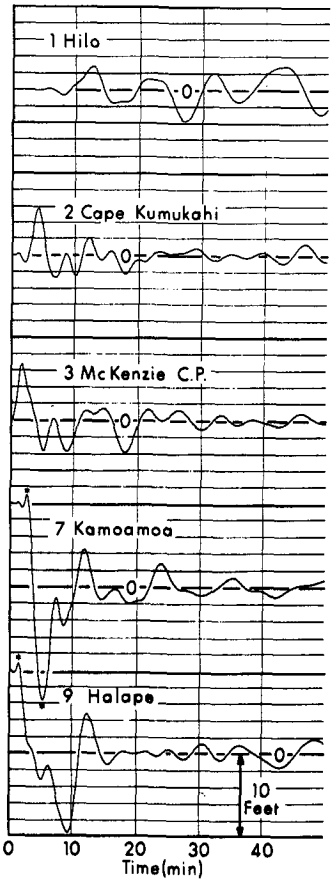

FIG. 3.

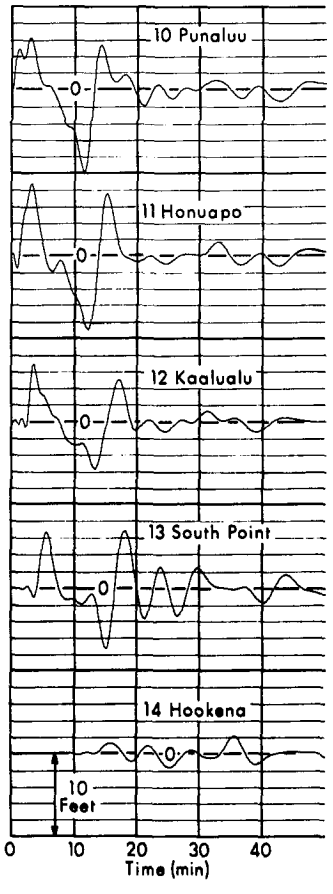

FIG. 4.

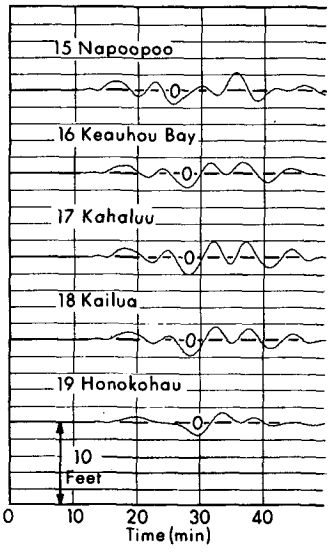

FIG. 5.

FIGS. 3–5. Predicted response for the 1975 Island of Hawaii tsunami at selected coastal sites. Outer boundary effects are for the most part absent for at least the first 40 min. The sequence of figures is in clockwise order starting at Hilo. Refer to Fig. 1 for precise locations. Small-scale differences in wave form are apparent over short distances. Asterisks at sites 7 and 9 refer to numerical overshoots and undershoots as discussed in the text.

2 to account for wave runup. As discussed in Section 2 the shoreline is assumed to be a fixed reflecting boundary. Associated with such a boundary is an amplification factor of 2. In actuality the shoreline should be described by a moving boundary. Spielvogel (1975) shows that a moving boundary leads to a higher amplification factor. For the purpose of this simulation we use his results which gives an amplification of approximately four for the periods involved. Thus, to convert shoreline amplification to runup heights we multiply by a factor of 2 (the ratio of the two amplification factors).

This is not the best way of treating wave runup but it is a convenient tool for use with a linear model. A future extension of this model will hopefully incorporate a shoreline moving boundary condition. This will eliminate the need for the runup factor used here which is appropriate for some waves but not for all waves incident on the shoreline. A moving boundary condition will also be a factor which would amplify subsequent waves more than the initial wave. This could then match the observation in several locations of the second wave being the largest.

The response of coastal sites within the source region (Fig. 3, Kamoamoa and Halape) shows a slight overshoot and undershoot corresponding to the arrival of the outer edge of the initial displacement. This is due to the polynomial approximation of the step initial condition. Although this represents a modification of the tectonic source, its effects are easily accounted for. The resultant source still has a leading edge with a large (but not infinite) slope which is modeled quite well by the arrangement in Eq. (12) for the gradient term.

The simulation of an infinite ocean by averaging solutions corresponding to fixed (Dirichlet condition) and free (Neumann condition) outer boundaries seems to be quite appropriate for this impulsively started tsunami problem where only a limited time history is of interest. For coastal sites (2–13) in the vicinity of the source region the outer boundary acts as a good transmitter for roughly 40 min. At that time a small-amplitude oscillatory wave appears which is most likely caused by multiple reflections with the outer boundary. This supposition is based on 1) the growing oscillations especially apparent at stations 2 and 9 of Fig. 3 when wave amplitude should be decreasing; and 2) The correspondence with expected arrival times of multiple reflections. Multiple reflections (which occur at a later time than the primary reflection) cannot be eliminated with this pair of solutions. For other coastal sites the complete time histories (as shown) are for the most part devoid of outer boundary reflections of appreciable amplitude.

The response at coastal and offshore sites indicates that the majority of the tsunami energy resulting from this uplift is carried in two to three waves of periods ranging from 10 to 15 min. This period compares well with that recorded by the Hilo tide gage. This period is also consistent with the travel time across the initial displacement.

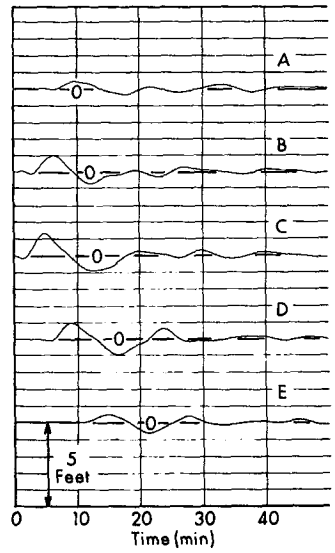

FIG. 6. Predicted response for the 1975 Island of Hawaii tsunami at selected deepwater sites. Outer boundary effects are for the most part absent for at least the first 27 minutes. Refer to Fig. 1 for precise locations. Comparison of amplitudes implies more energy is directed to the southwest.

Offshore sites (Fig. 6) indicate that more energy heads southwest than northeast. This feature is probably due to the bathymetry and source location.

Based on extensive surveys of Loomis (1975) and Tilling *et al.* (1976) of the runup of this tsunami around the island of Hawaii, Cox and Morgan (1977) have tabulated "accepted" wave runup heights. It is important to note that these are ranges of maxima and, thus, will include the superposition of the tsunami with shorter period wind waves and other shoreline oscillations. The ranges of these measured maxima at various sites are shown by the bars in Fig. 7. Also shown in Fig. 7 are maximum predicted wave runup heights resulting from the proposed Furumoto and Kovach initial displacement. Since our model only simulates long-period waves the predicted maxima will be up to 3 ft less than the measurements depending on the local conditions at the time of the tsunami.

It can be seen that the maxima for the Furumoto and Kovach source appear to be shifted too far northeast. This is an indication that their proposed uplift might be offset too far northeast or that it may be located correctly but is asymmetric with respect to its offshore axis. These possibilities would also help explain the discrepancies between

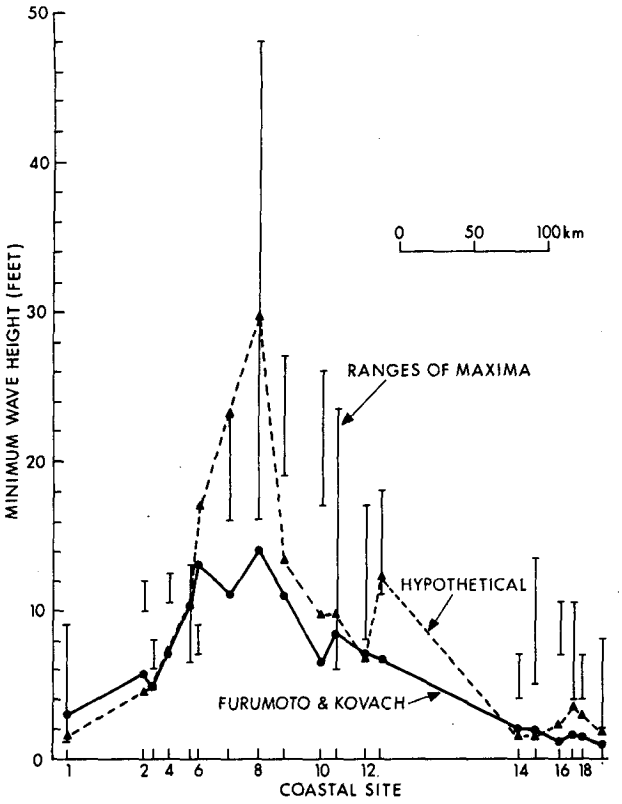

FIG. 7. Comparison of predicted and measured maximum wave heights at selected coastal sites. These are ordered left to right corresponding to a clockwise ordering from Hilo. See Fig. 1 for precise locations. Bars denote ranges of maximum wave heights measured at a particular site. General large-scale features are reproduced by the model.

observed and predicted wave arrival times (Fig. 8). The magnitude of the Furumoto and Kovach displacement also seems to be insufficient especially for sites in the source region (sites 7–10). A displacement of 7–10 ft would be necessary to give good correlation with the measurements.

In light of these differences a simulation was run for a hypothetical displacement (along the lines suggested by Ando, 1978 and Swanson *et al.*, 1976) of maximum amplitude 7.5 ft displaced offshore as shown in Fig. 2b. This uplift is again contained within the shaded region of Fig. 1 but its potential energy is roughly 85% that suggested by Furumoto and Kovach. Even so, the predicted maxima (also shown in Fig. 7) are greater in the source region and in better agreement with the measurements. This modification also improves the predicted shoreline wave arrival times (Fig. 8).

Further experiments with the source mechanism would undoubtedly lead to better correlation between predicted and measured wave heights and arrival times. Such features as the second wave being largest at some sites within the source region as well as at Hilo could also be obtained by shaping the initial displacement. This would be an approach to the "inverse problem" of inferring the ground motion given details of the resulting tsunami.

The question arises as to the applicability of the linear long wave equation in the source region. The nature of the source is the determining factor in the choice of governing equations. If the motion is of short duration and includes no large-amplitude slope, then the equations are valid. If these assumptions are violated, then there will be difference between the numerical model and the tsunami itself. Most of the differences will appear in the shape of the leading edge of the first wave. Since we are specifically interested in the peak amplitudes, there should not be significant difference in results between linear and nonlinear theories. Considering the distances and depths involved and the nature of the probable source mechanism, the wave equations should give proper peak amplitudes. The only nonlinearity which might contribute to the accuracy of the model is that which would be involved at the shoreline boundary condition. This has been discussed previously.

The fact that we can obtain good correlation between predictions and measurements for a particular uplift does not necessarily imply that

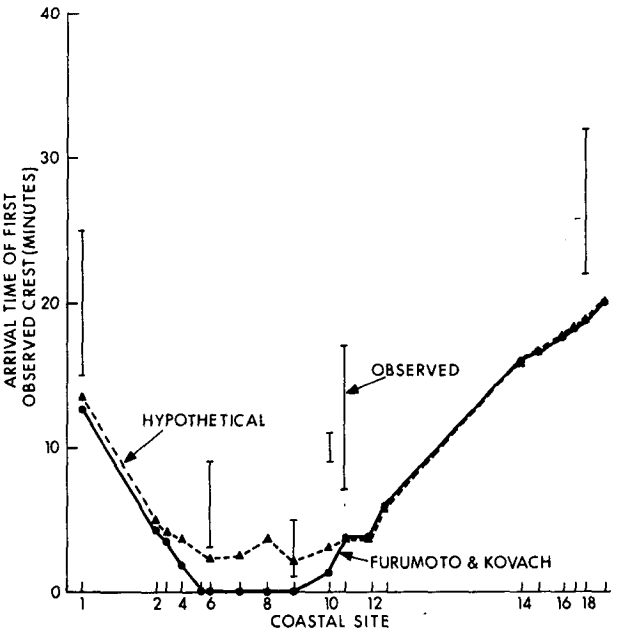

FIG. 8. Comparison of predicted and observed arrival times of first noticed crest at selected coastal sites. These are ordered left to right corresponding to a clockwise ordering from Hilo. See Fig. 1 for precise locations. Bars denote ranges of observations.

the uplift is the true ground motion. However, it does indicate that the uplift is acceptable as far as being a possible source mechanism.

The model also allows for the specification of an initial velocity ($\partial\eta/\partial t$) or for a moving ocean bottom. Simulations for an initial velocity of the source region rather than an initial displacement have been performed. Comparable magnitude wave heights are obtained for initial velocities of the order of 0.1 m s^{-1}. Here again the wave forms are found to be intimately dependent on the distribution of these velocities. Depending on the seismic source being considered, the initial condition, in general, should consist of some combination of displacement and velocity.

7. Conclusion

A time-stepping finite element scheme has been developed to study the transient response of a locally generated tsunami. The Galerkin method of weighted residuals leads to a straightforward matrix representation of the long-wave equation. The expected advantages of the FEM in handling irregular geometry and bathymetry are realized.

Simulations of the 1975 Hawaiian tsunami have demonstrated the practicality of the method. Inadequacies in the Furumoto and Kovach model have been illustrated and discussed. The present form of this fluid model will be used to test other tectonic theories of the 1975 Kalapana earthquake both in a direct and inverse manner. The latter together with measured wave heights should yield a good estimate of the location, center of mass and volume of the displaced sea bed at the time of the earthquake.

Other techniques to allow for a transmitting outer boundary as well as a moving shoreline boundary to incorporate wave runup are presently under investigation and will hopefully be included in future studies. With the addition of these features we should have an effective tool for predicting the shoreline response to arbitrary tsunamis.

APPENDIX

A Hybrid Linear-Quadratic Element

It has been established (Zienkiewiez, 1972) that quadratic surfaced finite elements can be used more cheaply and more accurately than linear elements to solve free surface gravity wave problems. There are anomalous cases where the opposite is true; one feature of the quadratic elements has been found to introduce occasional but serious errors and must be attended to in order to achieve uniformly good results. We will deal with the problem caused by the quadratic surface creating hills and valleys which are not indicated by data points. We will illustrate this point with a simple example of this anomaly by creating a quadratic surface and comparing the range of the surface to the range of the corresponding input nodal data. We will then generate a hybrid linear/polynomial surface to eliminate this error and finally relate this to the main paper.

Let us fit a quadratic surface using serendipity polynomials (Zienkiewicz, 1971) to a square element ($a \times a$) using the 8-point nodal data:

$$\{(\text{Depth, position, position})\} \equiv \{(h_d,x,y)\}$$
$$= \{(h_0 + \Delta h,\ 0,\ 0),(h_0,a/2,0),(h_0,a,0),(h_0,0,a/2),$$
$$(h_0,a,a/2),(h_0,0,a),(h_0,a/2,a),(h_0,a,a)\}.$$

The quadratic fit to this 8-node data is

$$h_q = h_0 - \Delta h\left(\frac{x}{a} - 1\right)\left(\frac{y}{a} - 1\right)\left(\frac{x+y}{a/2} - 1\right).$$

Let $\bar{\delta}$ represent the excursion of the quadratic surface beyond D, the range of nodal data, and let δ be the maximum excursion. More precisely

$$D = \{h \in [h_0,\ h_0 + \Delta h]\},$$
$$\bar{\delta}(x,y) = \text{MAX}\ \{[h_q(x,y) - \underset{\text{nodes}}{\text{MAX}}\ h_d],$$
$$[\underset{\text{nodes}}{\text{MIN}}\ h_d - h_q(x,y)],0\},$$
$$\delta \equiv \underset{\substack{x\in[0,a]\\ y\in[0,a]}}{\text{MAX}}\ \bar{\delta}(x,y),$$

where a non-zero δ indicates the presence of a hill or valley beyond the data range D.

Fig. A1 shows a plan view of this element illustrating that $\bar{\delta}$ is non-zero for over 87% of the element. In addition, $\bar{\delta}$ is at least $0.125\Delta h$ for 50% of the region and reaches the maximum $\delta = 0.25\Delta h$; that is, a 25% excursion beside the range of the data.

In this and other cases, problems in accuracy occur when one or more integration or interpolation points for the governing equation (wave equation for our models) coincide with nonzero $\bar{\delta}(x,y)$ excursions, in particular large $\bar{\delta}$ excursions. We note that higher order surfaces will generate anomalies of increasing magnitude.

The logical mathematical and computational solution to this problem would be to saturate such a region with many smaller elements. Unfortunately to do this increases the cost of computational time and also requires denser data sets and in general defeats the purpose for using quadratic (polynomial) surfaces.

A second method which we have found to be successful can be achieved at zero cost with no increase in computational effort. We create a mixed element which has both linear and quadratic sur-

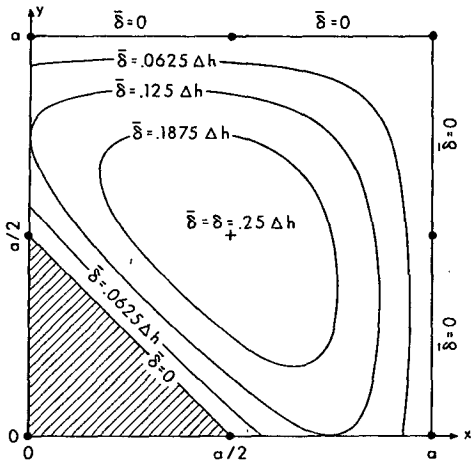

FIG. A1. Plan view of quadratic element fitting a quadratic surface to the 8-point nodal data of example 1. The 8 nodes are shown by solid dots. The hatched region shows $\bar{\delta} = 0$ where the quadratic surface lies within D, the range of the data. The clear region shows the creation of a hill where the quadratic surface lies outside of D. It is contoured up to the maximum value $\delta = 0.25\Delta h$.

faces. This is accomplished by truncating the surface ordinate at the integration points or interpolation points defined by the governing equation and the quadratic surface so as to always lie within the range of the nodal data for the same element, i.e., we redefine the depths h_q by demanding that $\bar{\delta} \equiv 0$ through the following procedure:

1) Establish array and nodal parameters.

2) Calculate h_{q_i}, the depths at the integration points for the governing equation based on parabolic surfaces h_q.

3) If

$$h_{q_i} > \underset{\text{(nodes)}}{\text{MAX}}\, h_d$$

then redefine

$$h_{q_i} \equiv \underset{\text{(nodes)}}{\text{MAX}}\, h_d.$$

4) If

$$h_{q_i} < \underset{\text{(nodes)}}{\text{MIN}}\, h_d$$

then redefine

$$h_{q_i} \equiv \underset{\text{(nodes)}}{\text{MIN}}\, h_d.$$

5) Procede to solve the system equations in the usual manner.

This is a rather simple fix but it does a substantial job. When no hills or valley are created by the quadratic element, this hybrid linear-quadratic element is identical to the quadratic element. When hills and valley are created, such as to extend beyond the range of the data, that part of the element is truncated with a plane surface. This fix becomes even more useful if we have a time-varying mesh. It allows us to alter our model without a costly constraint dependent on depth variations. If the anomaly occurs infrequently there is essentially no change in accuracy. If the anomaly occurs in many elements it is an indication that a denser set of elements is needed and this fix should not be used.

FLUID APPLICATION

We will use this method for evaluating the depth at the base of each element. The worst errors for the wave equation occur when this quadratic surface creates a hill in shallow water. The hill may even break the free surface causing the solution to diverge because of imaginary propagation speeds $(gh_q)^{1/2}$, where $gh_q < 0$ because of a non-negative depth h_q.

In solving tsunami problems, we are very interested in the wave behavior at the shoreline. In island and seamount models all the factors which generate the anomaly discussed above are present: 1) shallow water, 2) large changes in depth, 3) need for accuracy. The anomalies which cause singularities must be entirely eliminated. The large-scale picture of tsunami waves (main paper) is not terribly affected by several nonsingular anomalies of this type in the calculation scheme. Unfortunately, we need uniform accuracy at the shoreline where this anomaly does create significant errors (25% overshoots in wave heights, for example). It is for these reasons that this fix was chosen.

GENERAL APPLICATION

It is apparent that this anomaly will frequently appear in cases where polynomial elements are used in lieu of smaller linear elements in many physical problems. It is suggested that this hybrid surface is an efficient way of eliminating the anomaly at little cost to accuracy and computing time.

REFERENCES

Ando, M., 1978: The Hawaii earthquake of November 29, 1975: Low-angle normal fault due to forceful magma injection. U.S. Geological Survey. Unpublished.

Chen, M. H. T., 1973: Tsunami propagation and response to coastal areas. Inst. of Geophysics, Rep. HIG-73-15, University of Hawaii, 36 pp. + 39 figs.

Chen, H. S., and C. C. Mei, 1974: Oscillations and wave forces in an offshore harbour. Rep. 190, Ralph H. Parsons Laboratory for Water Resources and Hydrodynamics, MIT.

Cox, D. C., and J. Morgan, 1977: Local tsunamis and possible local tsunamis in Hawaii. Inst. of Geophysics, Rep. HIG-77-14, University of Hawaii, 118 pp.

Furumoto, A. S., and R. H. Kovach, 1977: Source mechanism study of the Kalapana earthquake of November 29, 1975. Part I. Body wave data. Inst. of Geophysics, University of Hawaii.

Hammack, J. L., 1972: Tsunami generation and near field propagation. Ph.D. thesis, California Institute Technology, 261 pp.

Hatori, J., 1976: Wave source of the Hawaii tsunami in 1975 and the tsunami behavior in Japan. Earthquake Research Inst., University Tokyo, No. 29, 355–363.

Houston, J. R., 1978: Interaction of tsunamis with the Hawaiian Islands calculated by a finite-element numerical model. *J. Phys. Oceangr.*, **8**, 93–102.

Hwang, L. S., and D. Divoky, 1970: Tsunami generation. *J. Geophys. Res.*, **75**, 6802–6817.

Kranzer, H. C., and J. B. Keller, 1959: Water waves produced by explosions. *J. Appl. Phys.*, **30**, 398–407.

Leendertse, J. J., 1967: Aspects of a computational model for long-period water wave propagation. Memo. RM-5294-PR, RAND Corp., 165 pp.

Loomis, H. G., 1975: The tsunami of November 29, 1975 in Hawaii. Inst. Geophysics, Rep. HIG-75-21, University of Hawaii, 29 pp.

Mader, C. L., 1974: Numerical simulation of tsunamis. *J. Phys. Oceangr.*, **4**, 74–82.

Reid, R. D., and A. C. Vastano, 1966: Orthogonal coordinates for the analysis of long gravity waves near islands. *Proc. Santa Barbara Specialty Conf. Coastal Engineering*, 1–20.

Smith, W. D., 1974: A nonreflecting plane boundary for wave propagation problems. *J. Comput. Phys.*, **15**, 492–503.

Spielvogel, L. Q., 1975: Single-wave run-up on sloping beaches. *J. Fluid Mech.*, **74**, 685–694.

Stoker, J. J., 1957: *Water Waves*. Interscience 467 pp.

Swanson, D. A., W. A. Duffield and R. S. Fiske, 1976: Displacement of the south flank of Kilauea Volcano: The result of forceful intrusion of magma into the rift zones. U. S. Geol. Survey Prof. Pap. 963, 39 pp.

Taylor, C., and J. Davis, 1974: Tidal and long wave propagation–A finite-element approach. *Comput. Fluids*, **3**, 125–148.

Tuck, E. O., and L. S. Hwang, 1972: Long wave generation on a sloping beach. *J. Fluid Mech.*, **51**, 449–461.

Zienkiewicz, O. C., 1971: *The Finite Element Method in Engineering Science*. McGraw-Hill, 521 pp.

——, 1972: Isoparametric and allied numerically integrated elements—A review. *Proc. ONR Int. Symp. Numerical and Computer Methods in Structural Mechanics*, A. Robinson, Ed., Academic Press.